Miner Deposita (2010) 45:583–597
DOI 10.1007/s00126-010-0293-8

ARTICLE

Fluid origin and structural enhancement during mineralization of the Jinshan orogenic gold deposit, South China

Xiaofeng Li · Chunzeng Wang · Renmin Hua · Xinglin Wei

Received: 25 February 2009 / Accepted: 31 May 2010 / Published online: 20 June 2010

Abstract The Jinshan orogenic gold deposit is a world-class deposit hosted by a ductile shear zone caused by a transpressional terrane collision during Neoproterozoic time. Ore bodies at the deposit include laminated quartz veins and disseminated pyrite-bearing mylonite. Most quartz veins in the shear zone, with and without gold mineralization, were boudinaged during progressive shear deformation with three generations of boudinage structures produced at different stages of progressive deformation. Observations of ore-controlling structures at various scales indicate syn-deformational mineralization. Fluid inclusions from pyrite intergrown with auriferous quartz have $^{3}He/^{4}He$ ratios of 0.15–0.24 Ra and $^{40}Ar/^{36}Ar$ ratios 575–3,060. $\delta^{18}O_{fluid}$ values calculated from quartz are 5.5–8.4‰, and δD values of fluid inclusions contained in quartz range between −61‰ and −75‰. The $\delta^{13}C$ values of ankerite range from −5.0‰ to −4.2‰, and ankerite $\delta^{18}O$ values from 4.4‰ to 8.0‰. The noble gas and stable isotope data suggest a predominant crustal source of ore fluids with less than 5% mantle component. Data also show that in situ fluids were generated locally by pervasive pressure solution, and that widespread dissolution seams acted as pathways of fluid flow, migration, and precipitation. The in situ fluids and fluids derived from deeper levels of the crust were focused by deformation and deformation structures at various scales through solution-dissolution creep, crack-seal slip, and cyclic fault-valve mechanisms during progressively localized deformation and gold mineralization.

Keywords Ductile shear zone · Gold deposit · Fluid origin · Noble gases · Stable isotopes · Progressive deformation · Jinshan

Editorial handling: N. White

X. Li (✉)
State Key Laboratory of Ore Deposit Geochemistry,
Institute of Geochemistry, Chinese Academy of Sciences,
Guiyang 550002, China
e-mail: x-f-li@hotmail.com

X. Li
Institute of Mineral Resources,
Chinese Academy of Geological Sciences,
Beijing 100037, China

C. Wang
University of Maine at Presque Isle,
Presque Isle, ME 04769, USA

R. Hua
Department of Earth Science, Nanjing University,
Nanjing 210093, China

X. Wei
Jiangxi Institute of Geological Exploration
for Mineral Resources of Nonferrous Metals,
Nanchang 330001, Jiangxi, China

Introduction

The Jinshan gold deposit, located in the northeast of Jiangxi Province, South China, is a world-class ductile shear zone-hosted gold deposit. The gold mining history at Jinshan dates back to the thirteenth century during the Song Dynasty. Massive gold ore bodies hosted by mylonites and with grades locally as high as 18 g/t were discovered at the deposit in the early 1980s. In the following 10 years, several other smaller deposits were discovered near Jinshan, including the Huaqiao and Bashiyuan gold deposits. More similar gold deposits such as Hamashi, Naikeng, and Dongjia, were discovered west of Jinshan in the 1990s. Proven gold reserves at the Jinshan deposit itself before its large-scale mining were estimated at 200 metric tons with

gold grades ranging from 4 to 20 g/t. Construction of a modern mining facility began in the early 1990s, and since 2005 the mine has processed an average of 5,000 metric tons of ore per day with annual yield of 5 metric tons of gold (equivalent to 176,370 ounces).

Extensive geologic research has been conducted in the area around the Jinshan deposit since the late 1980s. Previous workers have focused on relationships among the structural setting of the ore-bearing system, hydrothermal alteration, and mineralization processes (Ji et al. 1994a, b; Huang and Yang 1990; Zhu and Fan 1991; Wei 1995, 1996; Li et al. 2009), as well as on the origin of ore-forming fluids (Wei 1996; Wang et al. 1999a, b; Li et al. 2003). However, the origin of ore-forming fluids is still controversial and relationships between fluids and deformation processes and structures remain unclear (e.g., Hua et al. 2000; Li et al. 2003). For example, competing theories for the source of gold-related hydrothermal fluids based on $\delta^{18}O$, $\delta^{34}S$, and δD data, and Rb-Sr whole rock and mineral dating include (1) fluids released during metamorphic devolatilization of metasedimentary rocks (e.g., Wei 1996; Ji et al. 1994a); (2) hydrothermal fluids related to distal granite plutons (Huang and Yang 1990); and (3) formation water mixing with meteoric water (Wang et al. 1999b).

Progressively localized ductile shear zones evolved due to deformation softening and partitioning at shallow and middle crustal levels. They have most likely experienced prolonged progressive deformation and reactivation, and played an important role in the gold mineralization process. For example, they may serve as best candidate pathways for fluids and ideal locations for gold precipitation. Under certain conditions, in situ fluids generated in shear zones by pressure solution and diffusion-dissolution creep could play an important role in initiating mineralization process. The Jinshan ductile shear zone provides an excellent example for studying mechanisms of in situ fluid generation and evolution, as well as gold mineralization processes enhanced by gold-bearing fluids sourced from deeper levels of the crust.

In this study, macroscopic and microscopic deformation structures in the Jinshan ductile shear zone are analyzed to help understand mechanisms of in situ fluid generation, the geochemistry of deep-sourced fluids, and structural enhancement of the fluids during progressive deformation. Noble gases (He and Ar) in fluid inclusions from pyrite, carbon and oxygen isotope data from ankerite, oxygen isotopes of quartz, and hydrogen isotopes of fluid inclusions in quartz from high-grade ores, are studied to help reveal sources of ore-forming fluids.

Regional geologic and tectonic setting

The Jinshan gold deposit occurs within the Jiangnan (meaning "the south of Yangtze River") Orogenic Belt in northeastern Jiangxi Province. The Jiangnan Orogenic Belt records multi-stage Neoproterozoic orogenic events (Guo et al. 1980; Zhou and Zhu 1993; Charvet et al. 1996) caused by collision between the Huaiyu terrane in the southeast which belongs to the Cathaysia Block and the Jiuling terrane in the northwest which is part of the Yangtze Block, in Neoproterozoic time (Shu et al. 1995; Fig. 1a–c).

The Jiuling terrane is composed predominantly of continent-derived flysch turbidites and littoral sedimentary rocks of Mesoproterozoic to Neoproterozoic age. In its southern part, the flysch contains mafic and ultramafic intrusions dated at 1,515±241 Ma (Shu 1991). Past radiometric dating yielded several ages for Jiuling basement: tuffaceous phyllite Sm-Nd ages of 1,930±162 Ma and 700–800 Ma (Shu et al. 1989; Xu et al. 1992), and a zircon SHRIMP U-Pb age of 880 Ma (Wang et al. 2008). The Huaiyu terrane consists of Mesoproterozoic and Neoproterozoic metavolcanic rocks, including ophiolitic mélange dated at 930–1,000 Ma (Shu 1991), and turbiditic flysch. The volcanic rocks include mainly Mesoproterozoic basalt and diabase which show an affinity to oceanic or back-arc basin volcanics, and Neoproterozoic basalt, andesite, and rhyolite. These rocks are generally metamorphosed to greenschist facies except for a strip of blueschist facies ophiolitic mélange caused by the collision between the Huaiyu and Jiuling terranes (Shu and Zhou 1988). The age of the Huaiyu terrane ranges from 1,401 Ma (Rb-Sr on phyllite) to 700–800 Ma (Charvet et al. 1996). A dacite located at the top of the Huaiyu sequence gave a Rb-Sr isochron age of 817±83 Ma (Shu and Zhou 1988). The age data suggest that the collision between the Huaiyu and Jiuling terranes peaked in Neoproterozoic time. Intensive ductile thrust shearing and deformation subsequent to the collision took place mostly within the Huaiyu terrane during pre-Sinian times (Note: Chinese geologists refer the latest period of the Neoproterozoic as Sinian).

The presence of ophiolites, blueschist, and orogenic granites within the Jiangnan Orogenic Belt suggests an Alpine-style convergence between the Yangtze and Cathaysia blocks. Assembly of both blocks led to an angular unconformity in the sedimentary sequence of the Jiangnan Orogenic Belt along the southeastern margin of the Yangtze Block. In China, this Neoproterozoic orogenic event is named the Jinning orogeny. Charvet et al. (1996) suggested a multi-stage Neoproterozoic collision sequence, including early southeastward obduction and nappe emplacement at around 950±40 Ma, subsequent intrusions of S-type granitoids at 930±20 Ma, and an intracontinental shortening along some ductile shear zones.

The collision also resulted in regional shortening and folding of sedimentary rocks of the Shuangqiaoshan Group of the Jiuling terrane. A regional-scale synclinorium, the Sizhoumiao synclinorium, was produced parallel to the

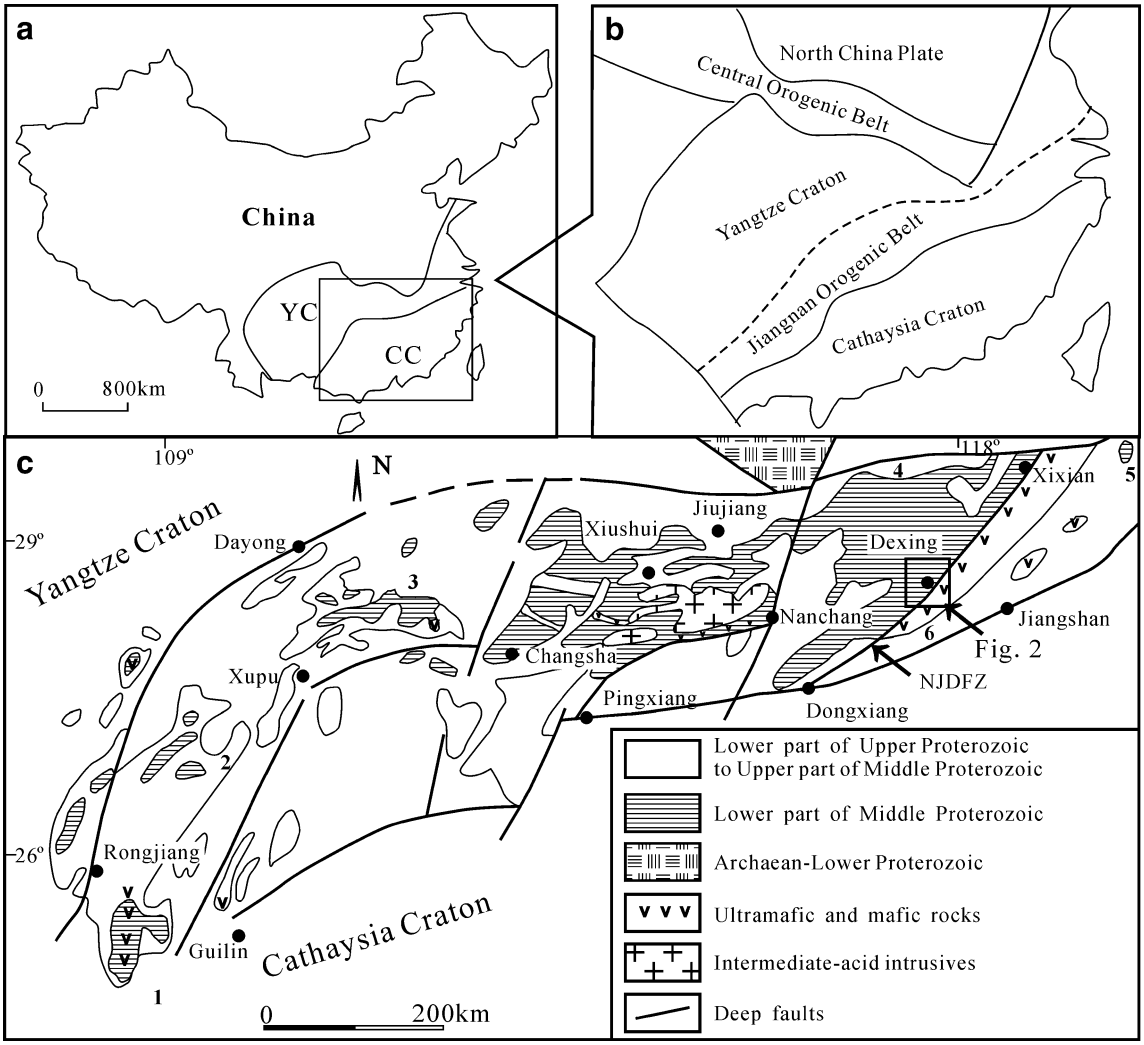

Fig. 1 **a** Simplified geologic map showing major tectonic units in south China. *YC* Yangtze Craton, *CC* South China Craton. **b** Major tectonic units in south China and surrounding areas. **c** Structural map of the Jiangnan Orogenic Belt with an emphasis on pre-Sinian geology (after Shu et al. 1995). (1) North Guangxi; (2) Southeast Guizhou; (3) North Hunan; (4) Jiuling terrane; (5) East Zhejiang terrane; (6) Huaiyu terrane

regional structures in the Group (Fig. 2). The collision was accompanied by regional greenschist-facies metamorphism indicated by newly formed chlorite and muscovite in the Shuangqiaoshan Group metasedimentary rocks.

The suture between the Huaiyu and Jiuling terranes is marked by a northeast-trending regional deep crustal fault system, the Northeast Jiangxi Deep Fault (NJDF) (Figs. 1c and 2). The NJDF is the dominant linear tectonic feature along the Jiangnan Orogenic Belt, extending continuously for at least 200 km from Dongxiang in Jiangxi Province northeastward to Xixian in Anhui Province. It dips steeply toward the northwest with a width ranging between 10 and 20 km. It is characterized by a 4–5-km-wide ophiolite and mélange sequence, including ductilely sheared Maoqiao ophiolite and Huaqiao mélange zones in the region (Fig. 2).

According to Shu (1991), the collision between Huaiyu and Jiuling terranes was dominated by oblique convergence and the strain was localized mostly in and around the NJDF. Strain partitioning led to development of several regional-scale, second-order northeast-striking high-strain zones such as the Bashiyuan-Tongchang and Jiangguang-Fujiawu ductile shear zones in the Jiuling terrane (Fig. 2). A series of nearly east-west-trending north-over-south thrusts such as the Jinshan ductile shear zone developed as a result of the oblique convergence. Because the shear zones occur within only pre-Sinian rocks, it is believed that the oblique convergence and subsequent ductile shearing took place during Mesoproterozoic to Neoproterozoic time. Geochronologic work on the Jinshan ductile shear zone such as a Rb-Sr whole rock age of 717±6 Ma (Zhang 1994), and Rb-Sr isochron ages of 714.5±60.5–732.1±61.9 Ma (Wei 1996) on the ultramylonite and mylonite produced in the ductile shear zones, confirms a Late Proterozoic Jinning age.

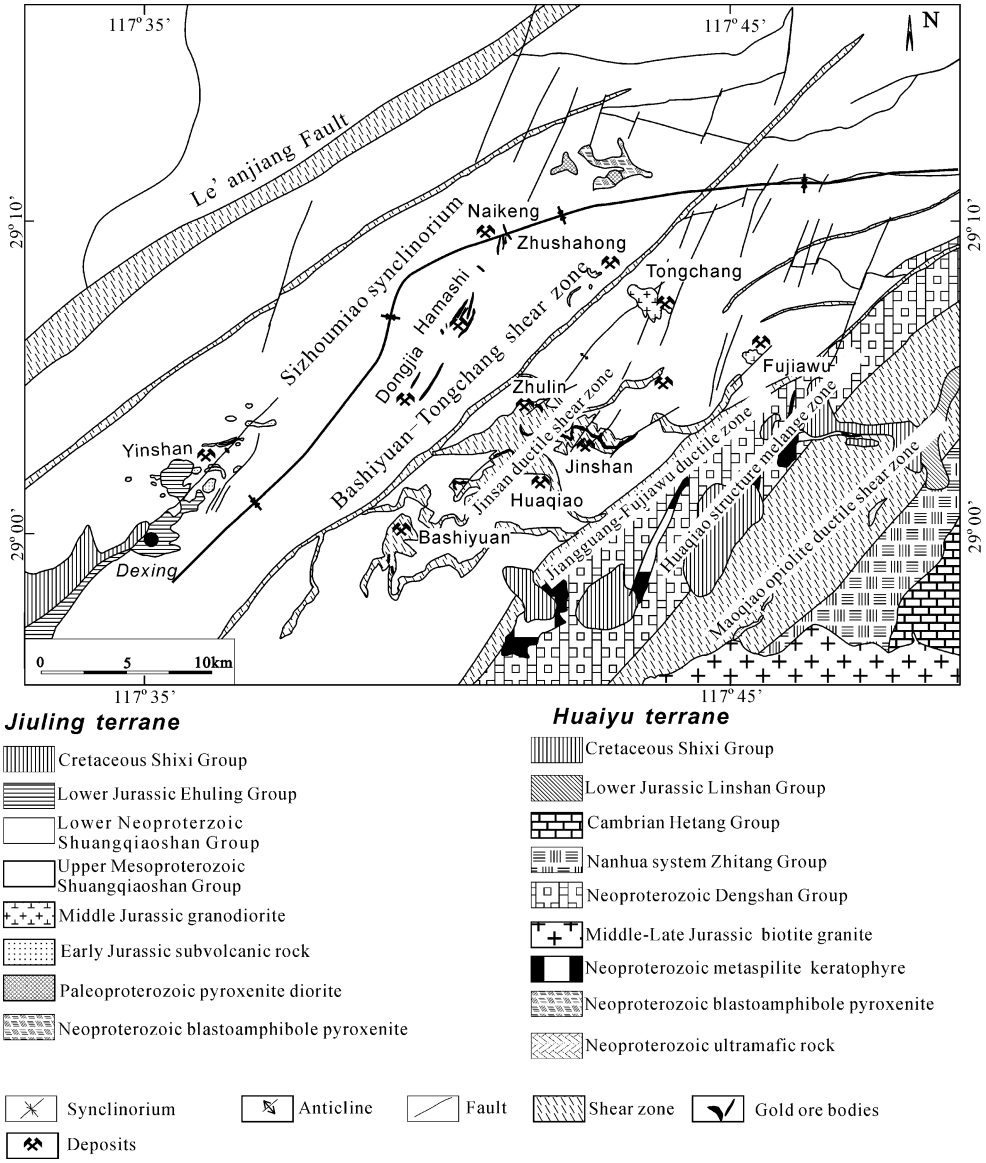

Fig. 2 Simplified geologic map of Jinshan gold deposit (modified after Wei 1996)

Shear zone control of ore formation

Like many other orogenic quartz vein gold deposits, Jinshan and other gold deposits in the region are closely associated with the NJDF, the first-order crustal-scale fault zone. In addition to the first-order NJDF, several second-order shear zones such as the northeast-striking Bashiyuan-Tongchang and Jiangguang-Fujiawu ductile shear zones are developed and serve as regional controls on lower order structures (Fig. 2) such as the third-order Jinshan, Xijiang, and Jinshankou shear zones, from the northeast to the southwest in the area. The third-order shear zones are as wide as 650 m, and dip shallowly to the northwest, north, and northeast at 5–30°. They directly host gold deposits such as Jinshan, Huaqiao, and Bashiyuan in the Neoproterozoic Shuangqiaoshan Group of slate, tuffaceous slate, phyllite, graywacke, and andesitic basalt dated at 880 Ma (zircon LA-ICP-MS, Wang et al. 2008; Fig. 2). As Fig. 2 shows, the third-order shear zones curve slightly as they merge with the second-order shear zones (Wei 1995). Kinematic studies of the third-order ductile shear zones reveal dominantly dip-slip motion with the south-southeast hanging walls thrust over the north-northwest footwalls (Wei 1995). They collectively show an imbricated pattern, indicating significant shortening during the Jinning orogeny.

Ore bodies at Jinshan are confined within the Jinshan ductile shear zone. The shear zone comprises sub-zones of mylonitized slate, protomylonite, mylonite, ultramylonite, and phyllitic mylonite due to intensive strain partitioning. The high-strain zone of ultramylonite, mylonite, and phyllitic mylonite coincides with the strongest hydrothermal alteration and gold mineralization in the deposit.

Mylonitic foliation in the shear zone is defined by alignment of dominant white mica or sericite and has a typical anastomosing fabric. The mylonite itself resembles typical fine-grained sericite-quartz schist. Detrital quartz grains show dynamic recrystallization and subgrain rotation. Quartz ribbons composed of subgrains of quartz are common. Quartz grains in laminated, auriferous quartz veins also display features of plastic deformation and dynamic recrystallization, indicating post-mineralization ductile shearing. New minerals such as sericite and chlorite dominate in the shear zone, suggesting greenschist–subgreenschist facies metamorphic conditions during the ductile deformation.

Pressure solution and diffusion-dissolution creep

Pressure solution is pervasive within the Jinshan shear zone. Quartz grains were dissolved at high stress surfaces where muscovite-defined foliation domains were in contact with quartz and where shear strain was high (Fig. 3a, b). Pyrite crystals with quartz pressure shadows are common in mylonite and phyllonite in the shear zone (Fig. 3c, d). Sericite was also precipitated in low-strain sites and became imbricated during subsequent progressive deformation.

Pressure solution and the associated diffusion-dissolution creep may play a more important role during deformation of shear zones than previously thought. According to van de Kamp (2008), pressure solution of quartz silt in shales may yield up to 6–9 wt.% SiO_2 at temperatures up to 200°C and a further 10–15 wt.% SiO_2 in the 200–500°C range. For muds altered to shales at 200°C, 14–20 wt.% silica is evolved and, a further 18–28 wt% silica is generated from 200°C to 500°C. Additional small amounts of silica may be released by alteration of feldspars to clays and stylolitization of quartz silt. Thus, voluminous silica-rich solutions could be released during intense pressure solution. In this study, we refer to the silica-rich fluids generated by pressure solution as in situ fluids that are thought to have precipitated within the ductile shear zone to form pyrite pressure shadows (Fig. 3c, d) and quartz veins.

In the Jinshan shear zone, quartz grains that were subjected to intense pressure solution include detrital quartz, quartz in some quartz veins precipitated in the early stage of ductile shearing, and fibrous quartz in pyrite pressure shadows (Fig. 3d).

Progressive deformation

Macroscopic and microscopic deformation structures observed in the Jinshan shear zone provide lines of evidence for a prolonged progressive deformation mechanism. Three generations of quartz vein boudinage structures have been identified in the shear zone, with each produced at a different stage of progressive shear deformation. The earliest is boudinage of quartz veins that were precipitated during the pressure solution and dissolution mass transfer described above. The boudinaged quartz veins parallel foliation and are sandwiched within schistose mylonite (Fig. 3e). Some of them have been stretched and folded into rootless folds.

The second generation of boudinaged quartz veins was produced during a later stage of ductile shearing. Their average thickness is greater than the first-generation quartz vein boudins and their quartz is typically milky white. They are parallel to foliation and are concentrated mostly within high-strain sub-zones of the shear zone. They differ from the first-generation quartz vein boudins in that they typically have a laminated structure (Fig. 3f), contain more sulfides such as pyrite, and host higher concentrations of gold. Most are mined as major ores. Quartz grains in the boudins are strongly ductilely deformed with significant development of plastic deformation structures.

The high-strain sub-zones are characterized by a network of second-order anastomosing ductile-brittle shear planes that are parallel or sub-parallel to the main shear zone boundaries. These secondary shear planes occur mostly along boundaries between competent and less competent lithologies, such as between pre-existing quartz veins and boudins and the much less competent schistose mylonite. Their anostomosing nature produced a system of boudinage structures with each boudin consisting of quartz veins (mostly pre-existing quartz vein boudins) and sheared schistose mylonite. These boudinage structures are attributed to the third generation of boudinage structures in the Jinshan shear zone, and occur mostly in high-strain sub-zones. The shear planes themselves are actually brittle fractures that contain thin layers of cataclasite, breccia, and gouge.

The three generations of boudinage structures are interpreted to represent a progressive deformation sequence from early ductile shearing to late-stage ductile-brittle deformation. The first and the second generations were produced by ductile shearing and accompanied by development of pervasive schistose foliation and stretching and flattening deformation structures, whereas the third generation was produced by ductile-brittle deformation with strain localization in high-strain sub-zones and on mostly the second-order shear planes.

Other lines of evidence for progressive deformation include pressure solution of quartz crystals precipitated at different stages of hydrothermal activity, and development of microscopic-scale ductile shear zones within aurifeous quartz veins. Microscopic-scale ductile shear zones are common in quartz veins produced in the main stage of gold mineralization and mined as high-grade ore. Quartz crystals subjected to strong plastic deformation and dynamic recrystallization are a

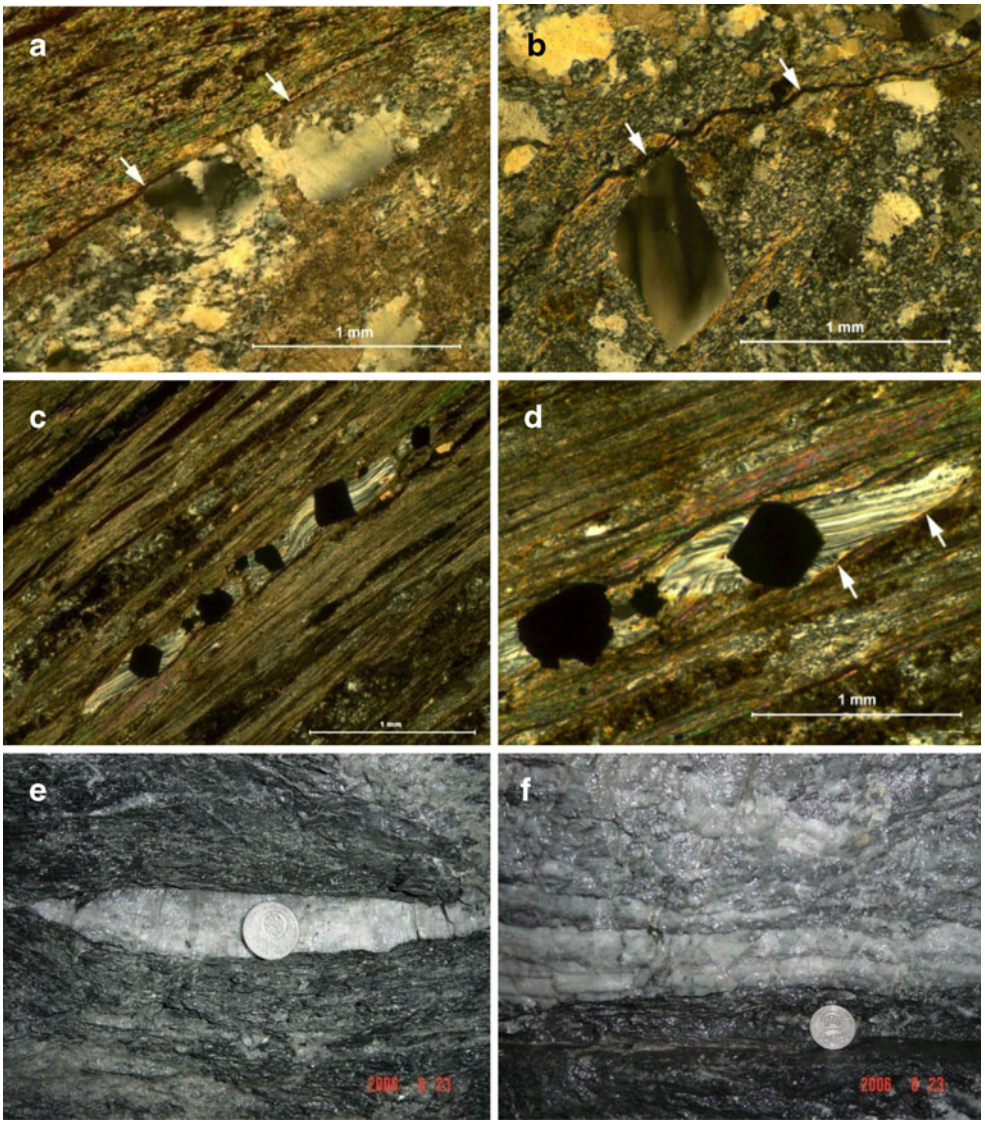

Fig. 3 Micro- and macro-structures of the sheared metasedimentary rocks and quartz veins. **a** and **b** Show typical pressure solution and dissolution seams. **c** A chain of pyrite crystals with quartz pressure shadows. **d** Pyrite with quartz pressure shadows showing dissolution of quartz fibers on shadow edge illustrating post-shadow pressure solution and progressive deformation. **e** A typical first-generation quartz vein boudin on an underground gallery wall. **f** Laminated gold-rich quartz vein on a gallery wall. All photomicrographs are under cross-polarizing light

characteristic feature of the laminated quartz veins, as are other microstructures such as subgrain rotation and deformation lamellae. In contrast, only a few of the feldspar clasts show kinking twins, and others were not affected at all by the shear deformation. These observations suggest that the temperature during deformation in the Jinshan shear zone was about 300–350°C (Passchier and Trouw 2000).

Ore geology and fluid inclusions

Most gold in the Jinshan deposit is concentrated in subordinate zones within the Jinshan shear zone and most ore bodies are either disseminated pyrite-bearing mylonite or laminated quartz veins. Disseminated ores around the laminated quartz veins contain 75% of the gold reserve, with ore grades ranging from 3 to 10 g/t Au. Ore grade is between 5 and 20 g/t Au in the quartz veins. High-grade ores are characterized by a greater abundance of base metal sulfides. Coarse, visible gold grains are commonly observed in hand samples and polished sections of laminated quartz veins. Native gold grains occur as irregular sheets, dendrites, and fine veinlets. High-grade pockets with grades in excess of 1,600 g/t Au have been reported (Wei 1995). Microscopically, native gold may appear as fine veins cutting fragmented pyrite crystals, as crack-filling veinlets within pyrite grains, or isolated in quartz grains (Fig. 4a, b). Intergrowth between native gold and pyrite has also been observed in quartz (Fig. 4b).

Ore bodies occur as lenses dipping to the northeast or north-northeast at 10–35°. The ore bodies are mostly parallel to shear planes and are 1.2 to 6.0 m thick with an average thickness of 3.5 m. Ore bodies are predominantly located at shear zone bends, dilational jogs, and contacts between rocks with different competencies. Boundaries between ore bodies and their host rocks are gradational and can only be determined with chemical analysis.

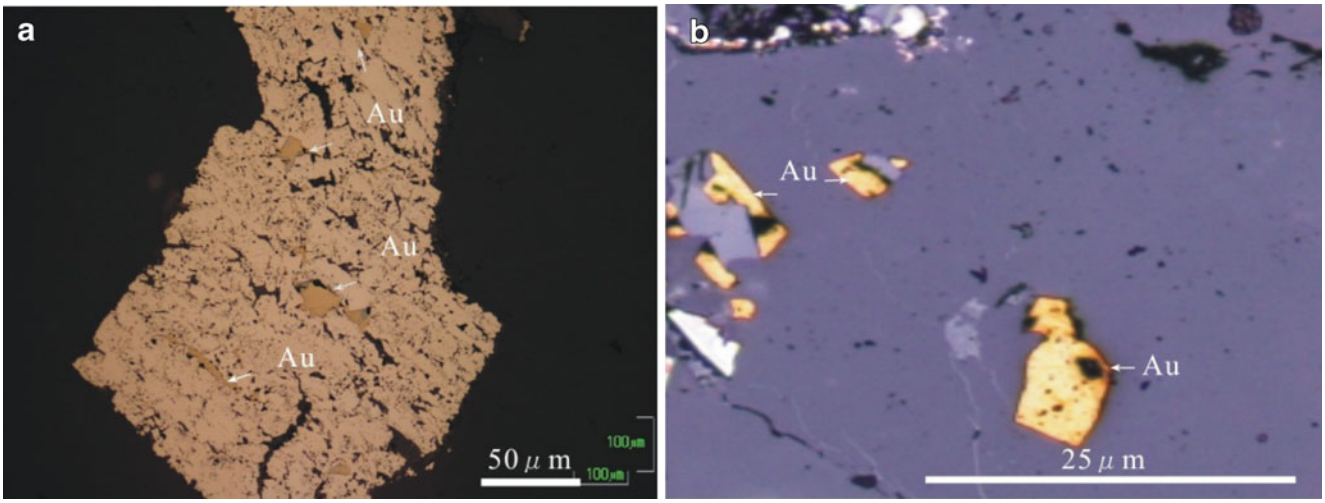

Fig. 4 Illustration of gold-quartz-pyrite associations. **a** Gold filling fractures in pyrite. **b** Gold occurring in quartz grains

Extensive hydrothermal alteration is closely associated with gold mineralization and includes silicic, pyritic, sericitic, and chloritic alteration. Three alteration zones have been identified from the center of the shear zone out to its wall rocks: (1) a quartz-albite-ankerite-pyrite zone that occurs in high-strain zones, (2) a quartz-sericite-ankerite zone next to the high-strain zones, and (3) a chlorite-calcite-sericite zone distal to the high-strain zones. The quartz-albite-ankerite-pyrite zone has width ranging from several meters to about 50 m and contains high-grade gold ores.

The mineralogy is relatively simple in both vein and disseminated ore types. Each contains less than three volume percent of sulfide minerals. The ore assemblage includes pyrite, pyrrhotite, arsenopyrite, sphalerite, chalcopyrite, ankerite, tetrahedrite, and native gold. Pyrite is dominant, typically representing more than 90% of the sulfides. Gold is contained in pyrite and quartz. The quartz-sericite-ankerite zone is up to 100-m wide but its ore grade is low. Ore minerals in the zone include pyrite, pyrrhotite, chalcopyrite, sphalerite, galena, and native gold. The chlorite-calcite-sericite alteration zone can be much wider, but does not extend beyond the limits of the shear zone.

Three mineralization stages have been identified: (1) Quartz-pyrite stage forming massive quartz and minor disseminated euhedral pyrite with low-grade gold. Gold occurs as microscopic inclusions in pyrite and alteration is dominantly silicic with minor pyritic alteration. (2) Quartz-sulfide stage forming sugary milky quartz, granular and veinlet pyrite, and minor galena, sphalerite, chalcopyrite, and arsenopyrite. This stage was the major mineralization stage accompanied by pyrite and ankerite. Mineral samples collected for noble gas and isotopic analyses formed in this stage. (3) The carbonate alteration stage is characterized by chlorite and calcite, with little gold mineralization.

Fluid inclusions in quartz from the quartz-sulfide stage of high-grade ores range from 5 to 20 μm in diameter and occur in round, oval, elongate, irregular, hook, and rare annular forms. In terms of textural and cross-cutting relationships, the fluid inclusions in quartz show three modes of occurrence: (1) in healed microcracks, (2) as three-dimensional clusters, and (3) along grain boundaries of plastically deformed quartz grains. The textural and cross-cutting relations as well as microthermometric data indicate that CO_2–H_2O liquid inclusions are most abundant at the deposit (Li 2001; Zhang and Tan 1998; Liu et al. 2005). Fluid inclusions can be homogenized and separated into gaseous and liquid phases, indicating boiling of the hydrothermal solution during the mineralization process. These fluids most likely represent the mineralizing fluids. The CO_2–H_2O fluids have salinities of 1–7 wt.% NaCl equivalent, and variable gas content. Their homogenization temperature is 300°C; they contain approximately 5 to 15 mol% CO_2 and 1 to 3 mol% N_2, as well as minor amounts of CH_4, CO, and H_2S (Zhang and Tan 1998; Li 2001; Liu et al. 2005).

Noble gas and stable isotopic compositions

Sampling and sample processing methods

Samples for noble gas and stable isotopic composition analysis were collected from five underground mining levels (50, 75, 100, 110, and 130 m). Quartz veins precipitated during the early stage of ductile deformation and associated with pressure solution described above were avoided. During sample preparation, quartz grains were not further classified due to lack of available CL microscopy. Samples collected from the quartz veins produced in the quartz-sulfide stage (the major gold mineralization phase)

include eight pyrite samples, seven quartz samples, and three ankerite samples. Pyrite occurs as anhedral and/or hypidiomorphic-granular assemblages; it may be intergrown with native gold and disseminated in quartz grains or in salvages. All the samples contain fluid inclusions associated with the major gold mineralization phase and exclude fluid inclusions possibly produced by pressure solution during the early stage of ductile deformation. Fluids associated with major gold mineralization in the later stage of deformation in the Jinshan shear zone could have originated from sources outside the shear zone. Quartz samples used in δD studies were carefully selected to maximize the percentage of primary CO_2–H_2O-rich fluid inclusions and the fluids were extracted by thermal decrepitation (Graupner et al. 2006). Quartz, pyrite, and ankerite grains were hand-picked from crushed vein and wall rock specimens under a binocular microscope. Samples were analyzed at the Stable Isotope Laboratory of the Institute of Mineral Resources, Chinese Academy of Geological Sciences.

He and Ar gases of fluid inclusions in pyrite were extracted using a vacuum crushing method as described in detail by Hu et al. (1998). He and Ar isotope concentrations were then measured with a Ukrainian MI-1201IG inert gas mass spectrometer. The standard gas concentration was measured and calibrated before analyzing the samples. The mass spectrometer was regularly calibrated against 1.32×10^{-7}cm^3 STP Ar with air ^{40}Ar/^{36}Ar, and 5.6×10^{-7}cm^3 STP He with ^{3}He/^{4}He $= 1.4\times10^{-6}$. All analytical results were based on the atmosphere standard, with ^{3}He/^{4}He of 1.4×10^{-6} (Ra), and ^{40}Ar/^{36}Ar of 295.5. The hot blank level of ^{4}He was 2×10^{-11}cm^3 STP, and the blank level for ^{40}Ar/^{36}Ar was 5×10^{-9}cm^3 STP.

Oxygen was liberated from quartz by reacting with BrF_5 (Clayton and Mayeda 1963) and converted to CO_2 on a platinum-coated carbon rod. The $\delta^{18}O$ determinations were made on MAT-253 mass spectrometer. Reproducibility for isotopically homogeneous pure quartz was about ±0.1‰ (1σ). Hydrogen isotope ratios on bulk fluid inclusions in quartz were measured by mechanical crushing of 5 g of quartz grains sized at 15 mm, following the method described by Simon (2001). Samples were first degassed of labile volatiles and secondary fluid inclusions by heating in vacuum to 200°C for 3 h. The degassed quartz was thermally decrepitated in an evacuated quartz tube inductively heated at >800°C. The released water was trapped, reduced to H_2 by zinc at 450°C, according to procedures adapted from Coleman et al. (1982), and then analyzed with the MAT-253 mass spectrometer. Analyses of standard water samples indicate precision of ±3‰ (1σ) for δD.

Carbon and oxygen isotope analyses of ankerite were obtained by using the phosphoric acid method (Hoefs 1987) at the Stable Isotope Laboratory of the Institute of Mineral Resources, Chinese Academy of Geological Sciences. The isotopic composition of CO_2 gas was measured by MAT-253 mass spectrometer with a precision of ±0.2‰. Carbon isotope ratios are reported relative to Peedee belemnite (PDB) standard and oxygen isotope ratios are reported relative to standard mean ocean water (SMOW).

Results

Noble gases The analysis results for noble gases He and Ar are listed in Table 1. The concentrations of ^{4}He range from 12.60 to 566.62×10^{-6}cm^{3}STP/g for all analyzed samples. ^{3}He/^{4}He ratios range from 0.13 Ra to 0.24 Ra (^{3}He/^{4}He ratios are given in units of the atmospheric ^{3}He/^{4}He ratios Ra $= 1.4\times10^{-6}$). The ^{40}Ar/^{36}Ar ratios are between 575 and 1,090 with exception of samples J08 and HQ-2, which have higher ^{40}Ar/^{36}Ar ratios (2,838 and 3,060, respectively). The ratios of ^{3}He/^{36}Ar show the greatest variability, ranging from 1.46×10^{-3} to 1.81×10^{-1}. The F^4He values (defined as $F^4He = \left(^4He/^{36}Ar\right)_{sample}/\left(^4He/^{36}Ar\right)_{air}$; e.g., Kendrick et al. 2001), which provide a good estimate of the atmospheric He contribution to the sample fluids, are $3.4\times10^4 - 5.1\times10^6$ for pyrite. $^{40}Ar^*/^4He$ ratios are from 0.01 to 0.05, lower than the crustal $^{40}Ar^*/^4He$ production ratios of 0.2 (Table 1).

Oxygen isotopes of quartz and hydrogen isotopes of fluid inclusions in quartz Seven quartz samples collected from high-grade ores that precipitated in the quartz-sulfide stage were analyzed for oxygen isotopes of quartz and hydrogen isotopes of fluid inclusions contained in quartz. The $\delta^{18}O$ values in quartz range from 12.4‰ to 15.3‰, and the δD values of water released from fluid inclusions in quartz range from −73‰ to −62‰ (Table 2).

Oxygen and carbon isotopes of ankerite As Table 3 shows, the $\delta^{13}C_{v\text{-}PDB}$ values of ankerite range from −5.0‰ to −4.2‰, whereas the $\delta^{18}O_{V\text{-}SMOW}$ values have a wide range from 4.4‰ to 8.0‰.

Discussions and conclusions

Sources and origins of the main mineralization phase ore fluids

Hydrogen and oxygen isotope compositions of hydrothermal minerals help constrain sources of ore-forming fluids. The $\delta^{18}O$ values of auriferous quartz veins at the Jinshan deposit are 12.4−15.3‰, close to the $\delta^{18}O$ values (14.5‰−15.2‰) of quartz contained in Au-poor quartz veins produced by earlier regional metamorphism. The

Table 1 Helium and argon isotopic data from fluid inclusions in pyrite at Jinshan gold deposit

Samples	Sample sites	$^3He/^4He$ ($\times10^{-7}$)	^4He ($10^{-6}cm^3STP/g$)	R/Ra	$^{40}Ar/^{36}Ar$	$^{40}Ar(10^{-7}cm^3STP/g)$	$^{40}Ar^*/^4He$	$^3He/^{36}Ar$	F^4He
J05	110 level; auriferous quartz vein with disseminated pyrite	2.57	232.39	0.19	575	23.52	0.05	1.46×10^{-3}	3.43×10^{4}
J08	130 level; auriferous quartz vein with disseminated pyrite, cross-cut by calcite vein	2.39	275.01	0.17	2,838	4.02	0.01	4.64×10^{-2}	1.17×10^{6}
J10	130 level; auriferous quartz vein with pyrite in selvage	3.35	76.10	0.24	869	5.70	0.05	3.89×10^{-3}	7.00×10^{4}
J14	50 level; auriferous quartz vein with disseminated pyrite	3.31	40.62	0.24	819	2.96	0.05	3.73×10^{-3}	6.80×10^{4}
J16	50 level; auriferous quartz vein with disseminated pyrite	1.80	147.91	0.13	1,090	2.60	0.01	1.12×10^{-2}	3.75×10^{5}
J20	100 level; auriferous quartz vein with disseminated pyrite	3.25	851.12	0.24	923	19.35	0.02	1.32×10^{-2}	2.45×10^{5}
HQ-1	75 level; auriferous quartz vein with disseminated pyrite	2.63	12.60	0.19	1,058	0.35	0.02	1.01×10^{-2}	2.32×10^{5}
HQ-2	75 level; auriferous quartz vein with disseminated pyrite	2.14	566.62	0.15	3,060	2.05	0.01	1.81×10^{-1}	5.11×10^{6}

δD values of fluid inclusions in the auriferous quartz veins vary from −62‰ to −73‰, overlapping the range between −80‰ and −40‰ that is typical for magmatic and/or metamorphic fluids (Rollinson 1993).

Pickthorn et al. (1987) and Goldfarb et al. (1989, 1991, 1997) suggested that δD values obtained from bulk extraction of fluid inclusions may not reflect primary ore-forming hydrothermal solutions, but rather represent secondary inclusions formed in the presence of surface meteoric water infiltrating the auriferous quartz veins. Their data from vein quartz of the Juneau mesothermal deposits showed that bulk extraction fluid inclusion water exhibit a wide range of δD values from -48‰ in relatively undeformed quartz to −110‰ in deformed counterparts. This wide span reflects decrepitation of variable proportions of two end-member fluids: primary ore fluids in primary inclusions and D-depleted meteoric water trapped in secondary inclusions in fractures. Samples analyzed in our δD study were selected from smaller quartz grains that show little deformation and that contain abundant CO_2-H_2O inclusions. Therefore, we believe the fluid inclusions in our samples consist dominantly of primary ore-forming fluids.

If extracted fluids are a mixture of metamorphic, heavy δD fluids with later, light δD meteoric fluids, then one should observe δD values that vary along a mixing line from meteoric to metamorphic δD values, depending on proportions of primary and secondary fluids collected. This phenomenon is, however, not observed in our samples. The δD values are relatively tight (±10‰) and show no trend toward metamorphic δD values (Fig. 5).

The $\delta^{18}O$ values of the fluids from all samples are calculated from the $\delta^{18}O$ values of hydrothermal quartz based on the trapping temperature of CO_2-H_2O fluid inclusions (300°C) by using the oxygen fractionation expression $1,000\ln\alpha Quartz-H_2O = 3.38\times10^6T^{-2}-3.4$ (Clayton et al. 1972). The values are 5.5–8.4‰. The oxygen and hydrogen isotope data for the Jinshan deposit are similar to those of Archean and Proterozoic lode gold deposits elsewhere in the world ($\delta^{18}O$= 6‰ to 11‰; δD=−30‰ to −80‰; McCuaig and Kerrich 1998). In the δD vs. $\delta\ ^{18}O_{H2O}$ diagram (Fig. 5), the data for the Jinshan deposit plot in a small field on the edge of the theoretical metamorphic fluid box, suggesting a metamorphic origin.

Carbon isotope composition of carbonates may potentially act as a tracer for sources of carbon. Carbon and oxygen isotope values of ankerite from auriferous quartz-sulfide veins formed during the main gold mineralization phase at Jinshan deposit in a range from −5.0‰ to −4.2‰ and from 4.4‰ to 8.0‰, respectively. These data are consistent with those for lode gold deposit of all ages, which encompass a large total spread of $\delta^{13}C$ values from approximately −23‰ to +2‰, but with individual deposits or camps tending to have much more restricted $\delta^{13}C$ values (McCuaig and Kerrich 1998)

Table 2 Oxygen and hydrogen isotopes composition in quartz of auriferous quartz veins

Sample	Mineral	$\delta^{18}O_{quartz}$	δD	$\delta^{18}O_{H2O}$
HQ-1	Quartz	15.3	−62	8.4
HQ-2	Quartz	13.2	−73	6.3
J08	Quartz	12.4	−65	5.5
J10	Quartz	14.6	−66	7.7
J13	Quartz	13.4	−73	6.5
J15	Quartz	14.9	−69	8.0
J20	Quartz	14.3	−68	7.4

Table 3 Carbon and oxygen isotope composition of ankerites from the inner alteration zone

Sample	Mineral	$\delta^{13}C_{V\text{-}PDB}$‰	$\delta^{18}O_{V\text{-}PDB}$‰	$\delta^{18}O_{V\text{-}SMOW}$‰
J08	Ankerite	−5.0	−22.9	7.3
J11	Ankerite	−4.2	−25.7	4.4
J18	Ankerite	−4.9	−22.2	8.0

(e.g., data from the Muruntau gold deposit showing a narrow range of values; $\delta^{13}C_{PDB}$, −4.9‰ to −8.5‰; $\delta^{18}O_{SMOW}$, 12.5‰ to 18.2‰; Graupner et al. 2006). The $\delta^{18}O$ values are not consistent with the data in the neighboring Dexing porphyry copper deposit ($\delta^{13}C_{PDB}$, −4.8‰ to −6.2‰; $\delta^{18}O_{SMOW}$, 6.8‰ to 18.8‰; Li and Sasaki 2007) and the Yinshan polymetallic deposit ($\delta^{13}C_{PDB}$, −7.6‰ to −4.3‰; $\delta^{18}O_{SMOW}$, 11.5‰ to 18.8‰; Jiangxi Geological Exploration Bureau 1996). Both the Dexing porphyry copper and Yinshan polymetallic deposits (see Fig. 2 for their location) are characterized by typical magmatic water involvement in their ore-forming process, whereas the Muruntau deposit is an example of mantle-derived fluids and/or lower-crust-derived fluids. The $\delta^{13}C$ value of ankerite ranges from −5.0‰ to −4.2‰ at Jinshan, suggesting that the carbon was probably derived from either a mantle or a metamorphic source.

The R/Ra ratios (R and Ra represent $^3He/^4He$ ratios in samples and the atmosphere respectively with $Ra = 1.4 \times 10^{-6}$) can be used to trace source(s) of helium contained in ore-forming hydrothermal solutions. The crust typically has an R/Ra ratio between 0.01 and 0.05 Ra (Tolstikhin 1978), which is much lower than that of the sub-continental lithospheric mantle that has an R/Ra ratio of 5–6 Ra (Dunai and Baur 1995). Mantle-derived fluids played an important role in some gold and copper ore systems, such as the Daduhe orogenic gold deposit in western China (Li et al. 2007), the Muruntau orogenic gold deposit in Uzbekistan (Graupner et al. 2006), the orogenic gold deposits of the Red River Gold Belt in Yunnan Province of China (Burnard et al. 1999), and the porphyry Cu deposits of the western USA (Kendrick et al. 2001).

Pyrite was regarded as an ideal mineral for trapping noble gases in fluid inclusions with the condition that it cannot be overprinted by any later hydrothermal activities (Baptiste and Fouquet 1996). The composition of fluids in quartz may be similar to that of pyrite where quartz intergrew with pyrite during the same ore-forming stage (Hu et al. 1998). At the Jinshan gold deposit, the measured He in fluid inclusions in pyrite cannot be the product of nuclear decay of lithium due to absence of Li-bearing minerals. Cosmogenic helium is not considered to be a source of ^3He either because all samples were collected from underground mine galleries (Simmons et al. 1987; Stuart et al. 1995). The atmospheric He contribution can be determined from the F^4He values, the $^4He/^{36}Ar$ ratio of the samples relative to the atmospheric $^4He/^{36}Ar$ value of 0.1655. Thus, a sample containing only atmospheric He has an $F\,^4He$ value of 1 (Kendrick et al. 2001). The F^4He values for our pyrite samples are much greater than 1, indicating that the pyrite-forming fluids contain negligible atmospheric He. All R/Ra values at the Jinshan gold deposit fall within a narrow range despite the broad concentrations of He, suggesting that diffusion and in situ ^4He production were not important in lowering R/Ra values (Craig and

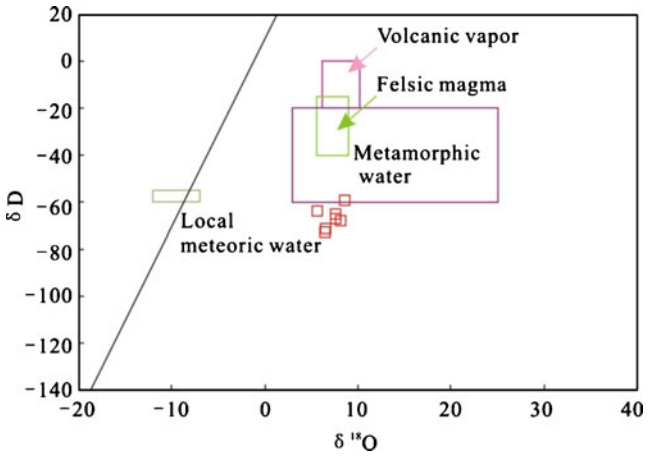

Fig. 5 δD vs. $\delta^{18}O_{H2O}$ diagram of fluids from auriferous quartz. The fields are simplified metamorphic fluids after Taylor (1974), mantle-derived fluids fields (Taylor 1974; Sheppard 1981), volcanic vapors, felsic magma, and magmatic water (Hedenquist and Lowenstern 1994)

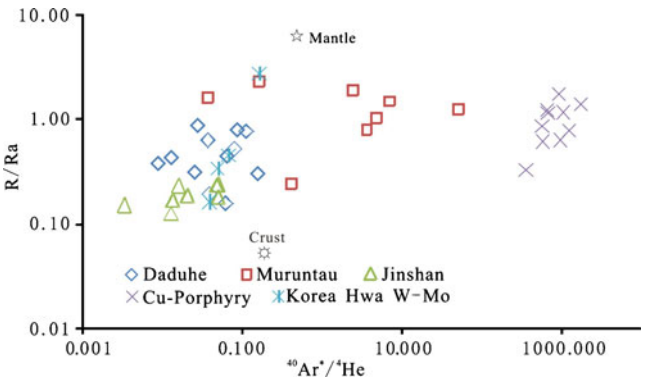

Fig. 6 $^{40}Ar^*/^4He$ vs. R/Ra diagram for fluid inclusions in pyrites. Estimates of the $^{40}Ar^*/^4He$ ratios for the crust (*white sun with rays*) and mantle (*white star*) are plotted on the figure. Data sources: Dae Hwa W-Mo deposit (Stuart et al. 1995), porphyry Cu deposits, USA (Kendrick et al. 2001), Daduhe Au deposit (Li et al. 2007), and Muruntau Au deposit (Graupner et al. 2006)

Lupton 1976). Liquid-rich and vapor-rich fluid inclusions were also observed and coeval within quartz grains (Zhang and Tan 1998). These samples should preserve a $^{3}He/^{4}He$ ratio close to that of fluids prior to boiling. Consequently, it seems unlikely that preferential vapor-phase fractionation of ^{3}He could account for the low He isotopic concentrations in gold-related pyrite. We therefore conclude that the He isotope data from fluid inclusions in pyrite from the Jinshan gold deposit represent the actual He isotopic composition of the hydrothermal fluids, and that the measured $^{3}He/^{4}He$ ratios (0.13–0.24Ra) result from the mixing of crustal and mantle reservoirs.

The R/Ra ratios can be used to estimate the proportion of mantle (Rm) and crustal (Rc) components in fluids. Using a value of 6 Ra as representative of pure mantle He (5–6 Ra), and 0.03 Ra as typical crustal fluids (0.01–0.05 Ra), a proportion of mantle He between 1.6 and 3.5% is estimated. This indicates that most He in the fluid inclusions in pyrite came from crustal sources. These data and analysis agree well with Sr isotope ratios of the strongly altered and deformed phyllite at Jinshan ($(Sr^{87}/Sr^{86})_o$=0.7082; Wei 1996; Wang et al. 1999b), which indicates a crustal strontium source.

The measured $^{40}Ar/^{36}Ar$ values of fluid inclusion gases extracted from pyrite range from 575 to 1,090 except samples J08 and HQ-2. These two samples have abnormal $^{40}Ar/^{36}Ar$ values; the reason is not clear. Compared with low atmospheric values (298), the higher $^{40}Ar/^{36}Ar$ values indicate a significantly higher concentration of $^{40}Ar^{*}$ (radiogenic ^{40}Ar) of mantle or crustal sources.

The $^{40}Ar^{*}/^{4}He$ values are between 0.01 and 0.05, much lower than the crustal $^{40}Ar^{*}/^{4}He$ production ratio of 0.2. The $^{40}Ar^{*}/^{4}He$ vs. R/Ra plot (Fig. 6) constitutes a well-defined correlation, suggesting that processes not yet fully understood may account for the variations in $^{40}Ar^{*}/^{4}He$ and $^{3}He/^{4}He$ ratios. The variations of $^{3}He/^{4}He$ and $^{40}Ar^{*}/^{4}He$ ratios imply mixing between mantle- and crust-derived fluids. The lower $^{40}Ar^{*}/^{4}He$ ratios also indicate that the crust-derived fluids dominated the gold mineralization process. In the $^{40}Ar/^{36}Ar$-$^{3}He/^{36}Ar$ plot (Fig. 7), an increasing influence of a metamorphic fluid component can be observed to characterize the pyrite. Because there was probably only a minor mantle source component involved in the gold mineralization process, and the $^{40}Ar/^{36}Ar$ value for the atmosphere is 298, it is suggested that the radiogenic ^{40}Ar may be derived from metamorphic processes.

The helium and argon isotope data therefore indicate that the ore-forming fluids had a dominantly crustal origin with little mantle association. In addition, atmospheric water shows little effect in the gold mineralizing fluids. The hydrogen and oxygen data alone cannot help discriminate between fluids of magmatic and metamorphic origins and determine which was primarily involved in the mineralization process. The carbon and oxygen isotope data from

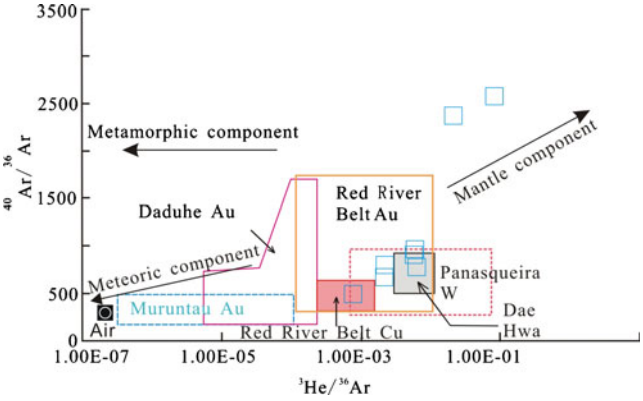

Fig. 7 $^{40}Ar/^{36}Ar$ vs. $^{3}He/^{36}Ar$ diagram for fluid inclusions in pyrite. Data sources: Panasqueira W deposit (Burnard and Polya 2004), Red River Belt Au deposits (Burnard et al. 1999), Red River Belt Cu deposits (Hu et al. 1998), others are the same as Fig. 6

ankerite suggest either a mantle component or a metamorphic origin. In summary, metamorphic fluids are the most likely candidate as the primary source of the main-phase ore-forming solutions at Jinshan deposit. This conclusion is consistent with studies conducted by previous workers (Zhang and Tan 1998; Li 2001; Wei 1995, 1996).

Structural enhancement of fluids

Structural enhancement of in situ fluids

As described previously, pressure solution is common and pervasive in the Jinshan shear zone. Silica-rich fluids were generated in situ by pressure solution. Pressure solution in the Jinshan shear zone was accompanied by intensively and pervasively developed dissolution seams (stylolites; Fig. 3a, b). Development of dissolution seams could significantly enhance porosity and permeability of the shear zone rocks, and provide pathways for migration of ore-forming solutions as well as space for silica precipitation. Their widespread presence indicates that diffusion mass transfer was an important deformation mechanism during the shear deformation process.

The silica released during Jinshan ductile shearing could precipitate as pyrite pressure shadows without much migration. However, most of the silica-rich solution may have migrated through the shear zone and been precipitated at low-pressure sites to form quartz veins. The quartz veins are generally white and have thickness ranging from sub-centimeter to several tens of centimeters and contain few pyrite or other sulfide grains. Because generation of and precipitation from the silica-rich solution took place during progressive shear deformation processes, the quartz veins occur dominantly parallel to foliation, forming typical syn-deformational quartz veins. The quartz veins were significantly sheared and boudinaged by stretching and flattening during subsequent shear deforma-

tion so shear bands and plastic deformation of quartz within the quartz veins are common.

Metamorphic differentiation conventionally refers to separation of an originally homogeneous rock into bands of contrasting mineralogy during metamorphism. Quartz veins without much mineralization contained in most metamorphic rocks are commonly attributed to metamorphic differentiation. Here we propose that pressure solution, dissolution mass transfer, and precipitation of quartz veins observed in the Jinshan shear zone were associated with metamorphic differentiation in the shear zone. Analyses of O and H isotopes contained in the quartz veins suggest an association of silica with the metamorphic differentiation process (Hua et al. 2002). The microstructural observations described here provide direct evidence for the association.

Measurements of gold content in the host Shuangqiaoshan Group by previous workers (e.g., a reported content of 15.30 ppb by Jiangxi Nonferrous Geological Survey 1989) yielded anomalously high background values, pointing to the Shuangqiaoshan Group as a source of the gold. If it is true, the possibility that widespread pressure solution could facilitate gold release from the host metasedimentary rocks cannot be excluded even if it could hardly produce a 200-tonne gold deposit itself. In this initial gold enrichment mechanism, the released gold could be incorporated into the solution/fluids and later precipitated with the quartz veins, though the veins may not be economically viable. This scenario is supported by pyrite sulfur data that shows that the $\delta^{34}S$ values of pyrite from high-grade ores are to the same as those of pyrite from the wall rocks of the shear zone (Wei 1996; Ji et al. 1994a). This equivalence demonstrates an in situ source of the ore-forming sulfur.

In summary, in situ silica-rich fluids are thought to have been generated during early ductile shearing in the Jinshan shear zone and later precipitated as quartz veins. Pressure solution and dissolution mass transfer may have facilitated initial gold enrichment in the shear zone, laying a foundation for subsequent large-scale gold mineralization. Subsequent progressive deformation and mineralization in the shear zone would continuously enhance gold enrichment and finally produce an economic gold deposit.

Structural enhancement of deep-sourced fluids

Progressive deformation in the Jinshan shear zone involved a transition from ductile deformation characterized by penetrative schistosity-dominated fabric to ductile-brittle deformation characterized by a non-penetrative (at outcrop and microscopic scales) network of sub-order shear planes. Development of the sub-order shear planes must have facilitated activation, migration, and enrichment of ore fluids from deeper levels of the crust. They could have acted as pathways of fluids and provided space for mineral deposition as evident from precipitation of gold-bearing pyrite. The existence of the second-generation quartz vein boudins indicates that a large amount of gold-bearing, silica-rich fluid was produced and precipitated during subsequent progressive ductile deformation. Boudinaged auriferous quartz veins of the second and the third generations indicate continued ductile and ductile-brittle shear deformation during and after main-phase emplacement of the quartz veins and gold mineralization.

Higher grade quartz veins in the deposit are always veins that show laminated structure (Fig. 3f). As suggested by Sibson (1986), lamination may be produced by a crack-seal slip mechanism involving prolonged slip due to repeated foliation opening, accompanied by fluid filling and mineral precipitation. Gold and hydrothermal minerals such as pyrite, chlorite, and sericite have been observed precipitated on slip surfaces in the laminated quartz veins.

Opening of the slip surfaces could have been caused by cyclic seismic displacement along the shear zone, with a high-strain rate during the later stage of brittle deformation. However, plastic deformation of quartz observed to be widespread in the laminated quartz veins indicates that the shear zone deformation was not completely brittle after the change in deformation regime. The repeated seismic slipping and opening could be controlled by fluctuations of fluid pressure with changes in or interplay between hydrostatic pressure and lithostatic pressure (Sibson 1987; Sibson et al. 1988).

Repeated slipping, opening, and sealing facilitated movement of and precipitation from ascending gold-bearing fluids. The fluids involved in the gold mineralization may have been generated by metamorphism and deformation at deeper levels of the crust; the regional deep first- and second-order shear zones very likely provided pathways for the ascent of the fluids into lower order ore-controlling shear zones such as the Jinshan shear zone. As discussed above, our noble gas and stable isotope studies show that the Jinshan ore fluids were dominantly related to metamorphic fluids. While the gold-rich fluids locally precipitated minerals to produce the laminated auriferous quartz veins, they were also dispersed throughout the mylonite and ultramylonite adjacent to the quartz veins producing the disseminated ore that makes up the bulk of the gold reserve in the deposit.

In summary, precipitation of gold from deeply sourced fluids into preexisting quartz vein systems was directly associated with and strongly enhanced by deformation processes and deformation structures. Gold mineralization was facilitated by localized processes within high-strain sub-zones where crack-seal slip mechanisms predominated.

A metallogenic model for Jinshan gold deposit

As stated by McCuaig and Kerrich (1998), orogenic gold deposits are generated at mid-crustal (4–16 km) levels proximal to accretionary terrane boundaries in transpressive subduction-accretion complexes of Cordilleran style orogenic belts. The Jinshan gold deposit occurs where two terranes, the Huaiyu and Jiuling terranes, collided during the Late Proterozoic Jinning orogeny, followed by transpressional or oblique accretion that caused along-orogen shearing. The large-scale shearing produced regional ductile shear zones at different scales. The deposit sits next to the first-order NJDF system and is intercalated by two second-order ductile shear zones, the northeast-striking Bashiyuan-Tongchang and Jiangguang-Fujiawu ductile shear zones.

Mineralization ages obtained for the Jinshan deposit by a number of workers using different geochronological methods are not consistent but range from Neoproterozoic to Mesozoic (e.g., Zhu and Fan 1991; Zhang 1994; Shu et al. 1995; Wei 1996; Wang et al. 1999b; Li 2001; Mao et al. 2008). Our interpretation is that the Jinshan gold deposit was produced in Neoproterozoic time during the Jinning orogeny as indicated by most workers (Zhu and Fan 1991; Zhang 1994; Shu et al. 1995; Wei 1996), and confirmed by the ^{40}Ar-^{39}Ar age of muscovite collected from gold-rich laminated quartz veins from Jinshan, which also indicated Neoproterozoic gold mineralization (Li, unpublished data). The structural relationships and the Neoproterozoic age demonstrate that the main phase of gold mineralization occurred after the peak of regional metamorphism that was associated with the Jinning orogeny, and the Jinshan gold deposit is a typical orogenic gold deposit as defined by Groves et al. (1998, 2000, 2003) and Goldfarb et al. (2001).

The first-order, crustal-scale NJDF served as a major channel for upward migration of the deeply generated fluids. Because the Jinshan ductile shear zone is located on the northwest side and in the hanging wall of the NJDF (Fig. 2), any deep-sourced fluids that traveled through the NJDF system would very likely move upwards into the sub-order Jinshan shear zone. As discussed, the deep-sourced fluids were predominantly metamorphic fluids produced at deeper levels of the crust, however, fluids generated in situ by significant pressure solution throughout the ductile shear zone cannot be excluded. Fluids generated either by in situ pressure solution or sourced from deeper levels of the crust must have been enhanced by deformation and deformation structures at various scales through solution-dissolution creep, crack-seal slip, and cyclic fault-valve mechanisms at different mineralization stages.

Acknowledgements This study was financially supported by the National Natural Science Foundation of China (grant number 40872065, 40403006, and 40610404013) and One Hundred Person Project of the Chinese Academy of Science. We are grateful to Richard Goldfarb, Patrick Williams, Craig Hart, and Noel White for their constructive reviews and significant help in improving the original manuscript. We thank Allan Ludman for his help in revising and improving English grammar. We also thank Kaiping Zhang and Xiankui Yi for their assistance during our field seasons.

References

Baptiste PJ, Fouquet Y (1996) Abundance and isotopic composition of helium in hydrothermal sulfides from the East Pacific Rise at 13°N. Geochim Cosmochim Acta 60:87–93

Burnard PG, Polya DA (2004) Importance of mantle derived fluids during granite associated hydrothermal circulation: He and Ar isotopes of ore minerals from Panasqueira. Geochim Cosmochim Acta 68:1607–1615

Burnard PG, Hu R, Turner G, Bi XW (1999) Mantle, crustal and atmospheric noble gases in Ailaoshan gold deposits, Yunnan Province, China. Geochim Cosmochim Acta 63:1595–1604

Charvet J, Shu LS, Shi YS, Guo LZ, Faure M (1996) The building of South China: collision of Yangtze and Cathaysia blocks, problems and tentative answers. J Southeast Asian Earth Sci 13:223–225

Clayton RN, Mayeda TK (1963) The use of bromine pentafluoride in the extraction of oxygen from oxides and silicates for isotopic analysis. Geochim Cosmochim Acta 27:43–52

Clayton KN, O'Neil JR, Mayeda TK (1972) Oxygen isotope exchange between quartz and water. J Geophyl Res 77:3057–3067

Coleman ML, Shepherd TJ, Durham JJ, Rouse JE, Moore GR (1982) Reduction of water with zinc for hydrogen isotope analysis. Anal Chem 54:993–995

Craig H, Lupton JE (1976) Primordial neon, helium and hydrogen in oceanic basalts. Earth Planet Sci Let 31:369–385

Dunai TJ, Baur H (1995) Helium, neon and argon systematic of the European subcontinental mantle: implications for its geochemical evolution. Geochim Cosmochim Acta 59:2767–2783

Goldfarb RJ, Leach DL, Rose SC, Landis GP (1989) Fluid inclusion geochemistry of gold-bearing quartz veins of the Juneau Gold Belt, southeastern Alaska: implicatios for ore genesis. In: Keays RR, Ramsay WRH, Groves DI (eds) The geology of gold deposits: the perspective in 1988. Econ Geol Monogr 6:363–375

Goldfarb RJ, Newberry RJ, Pickthom WJ, Gent CA (1991) Oxygen, hydrogen and sulfur isotope studies in the Juneau gold belt, southeastern Alaska: constraints on the origin of hydrothermal fluids. Econ Geol 86:66–80

Goldfarb RJ, Miller LD, Leach DI, Snee LW (1997) Gold deposits in metamorphic rocks of Alaska. Mineral deposits of Alaska. Econ Geol Monogr 9:151–190

Goldfarb RJ, Groves DI, Gardoll S (2001) Orogenic gold and geologic time: a global synthesis. Ore Geol Rev 18:1–75

Graupner T, Niedermann S, Kempe U, Klemd R, Bechtel A (2006) Origin of ore fluids in the Muruntau gold system: constraints from noble gas, carbon isotope and halogen data. Geochim Cosmochim Acta 70:5356–5370

Groves DI, Goldfarb RJ, Gebre-Mariam M, Hagemann SG, Robert F (1998) Orogenic gold deposits: a proposed classification in the context of their crustal distribution and relationship to other gold deposit types. Ore Geol Rev 13:7–27

Groves DI, Goldfarb RJ, Knox-Robinson CM, Ojala J, Gardoll S, Yun C, Holyland P (2000) Late-kinematical timing of orogenic gold deposits and significance for computer-based exploration techniques

with emphasis on the Yilgarn block, Western Australia. Ore Geol Rev 17:1–38

Groves DI, Goldfarb RJ, Robert F, Hart CJR (2003) Gold deposits in metamorphic belts: overview of current understanding, outstanding problems, future research, and exploration significance. Econ Geol 98:1–29

Guo LZ, Shi YS, Ma RS (1980) The geotectonic framework and crustal evolution of South China. In: Scientific papers on geology for international exchange, 1. Geological Publishing House, Beijing, pp 109–116 (in Chinese with English abstract)

Hedenquist JW, Lowenstern JB (1994) The role of magmas in the formation of hydrothermal ore deposit. Nature 370:519–527

Hoefs J (1987) Stable isotope geochemistry. Springer, Berlin, p 201

Hu RZ, Burnard PG, Turner G, Bi X (1998) Helium and argon isotope systematics in fluid inclusions of Machangqing copper deposit in west Yunnan Province, China. Chem Geol 146:55–63

Hua RM, Li XF, Lu JJ, Chen PR, Qiu DT, Wang G (2000) Study on the tectonic setting and ore-forming fluids of Dexing large ore-concentrating area, northeast Jiangxi province. Adv Earth Sci 15 (5):525–533, in Chinese with English abstract

Hua RM, Li XF, Zhang KP, Qiu DT, Yang FG (2002) Geochemical features of ore-forming fluid in the Jinshan gold deposit, Jiangxi province. J Nanjing Univ (Natural Sci) 38(3):408–417

Huang HL, Yang WS (1990) Geological characteristics and genesis of Jinshan gold deposit in the northeastern Jiangxi province. Contrib Geol Mineral Resour Res 5(2):29–39, in Chinese with English abstract

Ji JF, Liu YJ, Sun CY, Qiu DT (1994a) Geochemical characteristics of two types of ores from Jinshan shear zone-hosted gold deposit, Jiangxi,—with discussion on genesis of two-stage mineralization. Geochim 23(3):226–234, in Chinese with English abstract

Ji JF, Sun CY, Zheng Q (1994b) The metallogenetic characteristics of auriferous quartz vein in the Jinshan shear zone type gold deposit, Jiangxi province. Geol Rev 40(4):361–367, in Chinese with English abstract

Jiangxi Geological Exploration Bureau (JGEB) (1996) Yinshan Cu-Pb-Zn-Au-Ag deposit in Jiangxi Province. Geological Publishing House, Beijing, p 380, in Chinese with English abstract

Jiangxi Nonferrous Geological Survey (1989) Metallogeny and prospection of Dexing-Leping mineral belt. Jiangxi Nonferrous Geological Survey, Nanchang, p 258

Kendrick MA, Burgess R, Pattrick RAD, Turner G (2001) Fluid inclusion noble gas and halogen evidence on the origin of Cu-porphyry mineralizing fluids. Geochim Cosmochim Acta 65:2651–2668

Li XF (2001) The geochemistry research on fluid flow at Jinshan gold deposit, Jiangxi, China. Ph.D. Disseration, Nanjing University (in Chinese with English abstract)

Li XF, Sasaki M (2007) The hydrothermal alteration and mineralization of Middle Jurassic Dexing porphyry Cu-Mo deposit, Southeast China. Resour Geol 57(4):409–426

Li XF, Hua RM, Mao JW, Ji JF (2003) A study of illite Kübler Indexes and chlorite crystallinities with respect to shear deformation and alteration, Jinshan gold deposit, East China. Resour Geol 53(4):283–292

Li XF, Mao JW, Wang CZ, Watanabe Y (2007) The Daduhe gold district at the eastern margin of the Tibetan Plateau: He, Ar, S, O and H isotopic data and their metallogenic implications. Ore Geol Rev 30:244–256

Li XF, Yi XK, Zhu HP (2009) Source of ore-forming fluids in Jinshan gold deposit of Dexing County: constraints from microstructures and stable isotopes. Miner Depos 28(1):42–52, in Chinese with English abstract

Liu ZY, Jin CZ, Wang RH (2005) Geochemical feature of fluid inclusion in Jinshan gold deposit, Jiangxi province. Miner Resour Geol 19(2):127–133, in Chinese with English abstract

Mao GZ, Hua RM, Long GM (2008) Discussion on the mineralogenetic epoch of the Jinshan gold deposit, Jiangxi Province—based on the quartz fluids inclusion Rb-Sr dating. Acta Geol Sin 82:532–539 (in Chinese with English abstract)

McCuaig TC, Kerrich R (1998) P-T-t-deformation-fluid characteristics of lode gold deposits: evidence from alteration systematics. Ore Geol Rev 12:381–453

Passchier CW, Trouw RA (2000) Microtectonic. Springer, Berlin

Pickthorn WJ, Goldfarb RJ, Leach DL (1987) Comment on "dual origins of lode gold deposits in the Canadian Cordillera". Geology 15:471–472

Rollinson HR (1993) Using geochemical data: evaluation, presentation, interpretation. Longman Scientific and Technical Press, Harlow, Essex, England, p 352

Sheppard SMF (1981) Stable isotope geochemistry of fluids. In: Rickard DT, Wickman FE (eds) Chemistry and geochemistry of solutions at high temperatures and pressures. Physics and chemistry of the earth, vol 13 and 14. Pergamon Press, New York. pp 419–445

Shu LS (1991) The late Proterozoic terrane tectonics and collision orogenic belt in the north Jiangxi, eastern China. Ph.D. thesis, Nanjing University. p 212

Shu LS, Zhou GQ (1988) The first discovery of the high-presurre minerals in the collage zone of proteroic terranes in northern Jiangxi and its tectonic significance. J Nanjing Univ 24:421–429 (in Chinese with English abstract)

Shu LS, Xiong YG, Li YL (1989) The main features and plate tectonic significance of the middle-late Proterozoic flysch in North Jiangxi. Jiangxi Geol 2:167–178

Shu LS, Shi YS, Guo LZ (1995) Plate and terrane tectonics in the middle segment of Jiangnan orogenic belt and its collision orogenic dynamics. Nanjing University Publishing House, Nanjing, p 236

Sibson RH (1986) Earthquakes and rock deformation in crustal fault zones. Ann Rev Earth Planet Sci 14:149–175

Sibson RH (1987) Earthquake rupturing as a mineralizing agent in hydrothermal systems. Geology 15:701–704

Sibson RH, Robert F, Poulsen KH (1988) High-angle reverse faults, fluid-pressure cycling, and mesothermal gold-quartz deposit. Geology 16:553–555

Simmons SF, Sawkins FJ, Schlutter BT (1987) Mantle-derived helium in two Peruvian hydrothermal ore deposits. Nature 329:429–432

Simon K (2001) Does δD from fluid inclusion in quartz reflect the original hydrothermal fluids? Chem Geol 177:483–495

Stuart FM, Burnard PG, Taylor RP, Turner G (1995) Resolving mantle and crustal contributions to ancient hydrothermal fluids: He-Ar isotopes in fluid inclusions from Dae W-Mo mineralization, South Korea. Geochim Cosmochim Acta 59:4663–4673

Taylor HP Jr (1974) The application of oxygen and hydrogen isotope studies to problems of hydrothermal alteration and ore deposit. Econ Geol 69:843–883

Tolstikhin IN (1978) A review: some recent advances in isotope geochemistry of light noble gases. In: Alexander EC Jr, Ozima M (eds) Terrestrial noble gases. Japan Sci Press, Tokyo, pp 33–62

van de Kamp PC (2008) Smectite-illite-muscovite transformations, quartz dissolution, and silica release in shales. Clays Clay Miner 56(1):66–81

Wang KY, Liang ML, Lu ZX (1999a) Geology and origin of the Jinshan gold deposit in Jiangxi province and discussion on its genesis. Geol Prospect 35(2):17–20, in Chinese with English abstract

Wang XZ, Liang HY, Shan Q, Cheng JP, Xia P (1999b) Metallogenic age of the Jinshan gold deposit and Caledonian gold mineralization in South China. Geol Rev 45(1):19–23, in Chinese with English abstract

Wang XL, Zhao GC, Zhou JC, Liu YS, Hu J (2008) Geochronology and Hf isotopes of zircon from volcanic rocks of the Shuangqiaoshan Group, South China: implications for the Neoproterozoic tectonic evolution of the eastern Jiangnan orogen. Gondwana Res 14:355–367

Wei XL (1995) The geological characteristics and geological metallogenesis of Jinshan gold fields. Miner Resour Geol 9(6):471–480, in Chinese with English abstract

Wei XL (1996) The geological characteristics of Jinshan shear ductile shear zone type gold deposit in Jiangxi province. Geol Jiangxi 10 (1):52–64, in Chinese with English abstract

Xu B, Guo LZ, Shi YS (1992) The Proterozoic terranes and multiphase collision-orogens in Anhui-Zhejiang-Jiangxi area. Geological Publishing House, Beijing, p 112, in Chinese with English abstract

Zhang JC (1994) Metallogenic geochemical study of the ductile shear zone-type Jinshan gold deposit of Jiangxi Province. Ph.D. Dissertation, Nanjing University (in Chinese with English abstract)

Zhang WH, Tan TL (1998) Relationship between organic fluids and gold mineralization in the Jinshan gold deposit, Jiangxi Province. Miner Depos 17(1):15–24, in Chinese with English abstract

Zhou XM, Zhu YH (1993) Late Proterozoic collisional orogen and geosuture in southeastern China: petrological evidence. Chin J Geochem 12(3):239–251

Zhu KJ, Fan HR (1991) The geological features and ore-forming condition in Jinshan gold deposit. J Nanjing Univ Earth Sci Ed 2:177–185 (in Chinese with English abstract)